

# Co–Co<sub>2</sub>C and Co–Co<sub>2</sub>C/AC Catalysts for Hydroformylation of 1-Hexene under Low Pressure: Experimental and Theoretical Studies

Wenda Dong,<sup>†,§,||</sup> Jinxun Liu,<sup>‡,§,||</sup> Hejun Zhu,<sup>†</sup> Yunjie Ding,<sup>\*,†,‡</sup> Yanpeng Pei,<sup>†,§</sup> Jia Liu,<sup>†,§</sup> Hong Du,<sup>†,§</sup> Miao Jiang,<sup>†,§</sup> Tao Liu,<sup>†</sup> Haiyan Su,<sup>‡</sup> and Weixue Li<sup>\*,‡</sup>

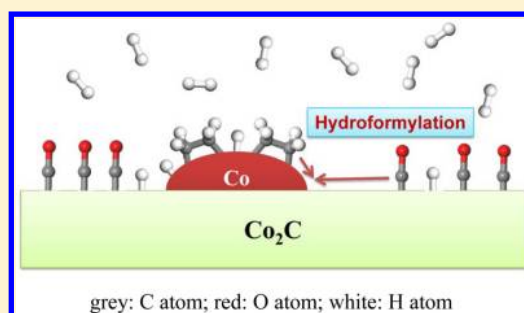
<sup>†</sup>Dalian National Laboratory for Clean Energy, Dalian Institute of Chemical Physics, Chinese Academy of Sciences, Dalian, 116023, China

<sup>‡</sup>State Key Laboratory of Catalysis, Dalian Institute of Chemical Physics, Chinese Academy of Sciences, Dalian, 116023, China

<sup>§</sup>University of Chinese Academy of Sciences, Beijing 100039, China

## S Supporting Information

**ABSTRACT:** Unsupported Co–Co<sub>2</sub>C catalyst and active carbon supported Co–Co<sub>2</sub>C (Co–Co<sub>2</sub>C/AC) catalysts were prepared and have been first proven to be highly active for 1-hexene hydroformylation under low pressure ( $P = 3.0$  MPa and  $T = 453$  K). It is found that the catalytic performances over the Co–Co<sub>2</sub>C and Co–Co<sub>2</sub>C/AC catalysts were strongly dependent on the ratio of Co<sub>2</sub>C to Co. Highly catalytic performances were achieved with the XRD intensity ratio of Co<sub>2</sub>C to Co ranging from 0.7 to 1.2. Co–Co<sub>2</sub>C/AC catalyst with carburization for 20 h has a highly catalytic stability for 1-hexene hydroformylation with a time stream of 140 h, indicating that no dissolved cobalt carbonyl species were formed and thus led to no cobalt elution during hydroformylation under reaction conditions. Density functional theory (DFT) calculations have been conducted to understand the nature of the catalytic performance. We found that the interface between Co and Co<sub>2</sub>C plays a significant role in ethylene hydroformylation. Metallic Co sites are used for olefin adsorption and activation to form surface carbonaceous species, while Co<sub>2</sub>C sites, for CO molecular adsorption, activation, and insertion. Our results have provided a strategy for designing highly active bifunctional non-noble metal catalysts.



## 1. INTRODUCTION

Hydroformylation reaction, catalyzed by transition metal complexes, involves the addition of hydrogen and carbon monoxide into a carbon–carbon double bond, yielding aldehydes in one-step fashion with 100% atomic economy.<sup>1</sup> Co-based and Rh-based complex catalysts, which are widely used in homogeneous hydroformylation with the advantage of their high catalytic activity and selectivity, are unfortunately difficult to separate from the products.<sup>2</sup> Therefore, a great number of studies have been conducted to deposit homogeneous Rh or other noble metal complexes on inorganic carriers for olefin hydroformylation.<sup>3</sup> In heterogeneous catalysis, supported cobalt catalyst employed as the catalyst for olefin hydroformylation has been reported, which opens a new avenue for reducing the usage of noble metal.

Compared to Rh-based catalyst, the supported cobalt catalyst has a lower activity and selectivity for olefin hydroformylation reaction. Nevertheless, it has been shown that the addition of a small amount of Pt, Pd, and Ru promoters in Co/SiO<sub>2</sub> could lead to a great improvement of catalyst activity and stability for hydroformylation of 1-hexene at 403 K and 5.0 MPa conditions.<sup>4</sup> Y. Zhang et al. have derived that noble metal promoted Co-based catalysts (supported by activated carbon, Co/AC), especially Rh-promoted Co/AC catalysts, were active

and selective for the olefin hydroformylation.<sup>5,6</sup> However, in the supported cobalt-based hydroformylation catalyst systems, some soluble cobalt carbonyl compounds were detected in the products; i.e., it was found that ca. 1 wt % cobalt was dissolved for various Co/SiO<sub>2</sub> catalysts after 2 h hydroformylation reaction in an autoclave reactor.<sup>7</sup> Furthermore, it was previously reported that some soluble Co species, such as cobalt carbonyls, could be formed and led to the elution of Co from the supported Co catalysts at 403 K.<sup>7–9</sup> The loss of Co could lead to the poor stability of hydroformylation reaction in the supported cobalt-based catalysts. Therefore, it is still a great challenge to obtain a heterogeneous supported cobalt catalyst with high performance of hydroformylation and good catalytic stability without elution of active metal species under hydroformylation reaction conditions.

Transition metal carbides have attracted much more attention in recent years due to their comparable performance to noble metals in many reactions including hydrogenation,<sup>10</sup> ammonia synthesis and decomposition,<sup>11</sup> hydrodesulfurization (HDS),<sup>12</sup> hydrodenitrogenation (HDN),<sup>13</sup> water–gas shift

Received: April 30, 2014

Revised: July 25, 2014

Published: July 29, 2014

reaction,<sup>14</sup> hydrocarbon isomerization,<sup>15</sup> etc. Among all the transitional metal carbides, cobalt carbide ( $\text{Co}_2\text{C}$ ) has not been taken notice in terms of catalysis. The formation of  $\text{Co}_2\text{C}$  is always considered as a possible deactivation cause or nonactive species during the Fischer–Tropsch (F–T) synthesis reactions.<sup>16–20</sup> However, it is thus surprising when Volkova proposed  $\text{Co}_2\text{C}$  as being able to activate CO without rupture and insert CO into carbonaceous intermediate species that could lead to the formation of higher alcohols ( $\text{C}_1$ – $\text{C}_6$  alcohols) over Co–Cu-based catalyst in CO hydrogenation reaction.<sup>21</sup> We have also previously reported that linear alcohols ( $\text{C}_1$ – $\text{C}_{18}$ ) could be directly synthesized via Fischer–Tropsch reaction from syngas (CO and  $\text{H}_2$  mixture) over the activated carbon supported Co-based catalyst containing metallic Co ( $\text{Co}^0$ ) and  $\text{Co}_2\text{C}$  species.<sup>22–25</sup> It is suggested that  $\text{Co}_2\text{C}$  plays a significant role in the selectivity for higher alcohols. We have derived a reaction mechanism that metallic  $\text{Co}^0$  was used for the dissociative adsorption of CO molecules, C–C chain growth and formation of  $\text{C}_n\text{H}_m$ –M species, and  $\text{Co}_2\text{C}$  was responsible for CO insertion into the  $\text{C}_n\text{H}_m$ –M species to form higher alcohols. Subsequently, Lebarbier carried out combined theoretical and experimental studies on the same catalysts as we used, and they found the catalysts with the highest  $\text{Co}_2\text{C}/\text{Co}$  ratios had the highest selectivity toward alcohols.<sup>26</sup> Since  $\text{Co}_2\text{C}/\text{Co}$ -based catalysts can provide the active sites for CO activation and insertion, whether these catalysts can also serve as an active catalyst for hydroformylation reaction is still unclear according to our knowledge.

In this work, we have synthesized  $\text{Co}_2\text{C}/\text{Co}$  catalysts to catalyze 1-hexene hydroformylation. To the best of our knowledge, it was the first time that the noble-like metallic Co– $\text{Co}_2\text{C}$  and active carbon supported Co– $\text{Co}_2\text{C}$  nanoparticles (Co– $\text{Co}_2\text{C}/\text{AC}$ ) were employed as the catalysts for the low-pressure hydroformylation of olefins. Moreover, DFT calculations have been performed to provide a mechanistic understanding for the olefin hydroformylation reaction on the Co– $\text{Co}_2\text{C}$ - and Co– $\text{Co}_2\text{C}/\text{AC}$ -based catalysts.

## 2. EXPERIMENTAL SECTION

**2.1. Preparation of the Catalysts.**  $\text{Co}_2\text{C}$  sample was prepared according to the following procedure:  $\text{Co}_3\text{O}_4$  was first reduced in the quartz reactor in a flow of  $\text{H}_2$  with a gas hourly space velocity of  $500\text{ h}^{-1}$  (GHSV =  $500\text{ h}^{-1}$ ) at 703 K and atmospheric pressure conditions. Then, the sample was cooled to 493 K and in the same flow followed by carburized with CO (GHSV =  $500\text{ h}^{-1}$ ) for 250 h at 493 K and 3.0 MPa before being quenched to room temperature and passivated in a flow of 1%  $\text{O}_2/\text{Ar}$ . The  $\text{Co}_2\text{C}$  sample was decomposed at 523 K and 0.1 MPa in a  $\text{H}_2$  flow (GHSV =  $500\text{ h}^{-1}$ ) for 2 h and passivated in a flow of 1%  $\text{O}_2/\text{Ar}$  at room temperature to prepare the one-step-decomposed Co– $\text{Co}_2\text{C}$  catalyst (the one-step-decomposed sample). The resulting one-step-decomposed sample was further decomposed at 543 K and 0.1 MPa in a  $\text{H}_2$  flow (GHSV =  $500\text{ h}^{-1}$ ) for 2 h and passivated in a flow of 1%  $\text{O}_2/\text{Ar}$  at room temperature to prepare the two-step-decomposed Co– $\text{Co}_2\text{C}$  catalyst (the two-step-decomposed sample).

The supported Co– $\text{Co}_2\text{C}/\text{AC}$  catalyst was prepared according to the following procedure. The catalyst precursor was first prepared by the method in which an aqueous solution of  $\text{Co}(\text{NO}_3)_2$  was impregnated on the activated carbon using incipient wetness impregnation techniques, and then dried at 333 K overnight in an oven. A 2 mL portion of the catalyst precursor was consequently loaded in the fixed-bed continuous-

flow (9.0 mm i.d.) stainless microreactor, and the catalyst was *in situ* synthesized in the reactor by the method demonstrated as follows: The sample was dried at 393 K for 4 h and then calcined at 623 K and 0.1 MPa for 4 h in a  $\text{N}_2$  flow (GHSV =  $500\text{ h}^{-1}$ ). After being cooled down to 393 K, the sample was reduced at 703 K and 0.1 MPa for 10 h in a  $\text{H}_2$  flow (GHSV =  $1000\text{ h}^{-1}$ ). After the sample was quenched to room temperature, the sample was then carburized at 493 K in a syngas flow ( $\text{H}_2/\text{CO} = 1:1$ , GHSV =  $500\text{ h}^{-1}$ ) at 3.0 MPa by tuning the carburization time (the carburization times were 0, 2, 20, 40, and 250 h, respectively). Prior to use, the activated carbon support (Tangshan Lianhe Activated Carbon Co. Ltd., BET surface area:  $780\text{ m}^2/\text{g}$ , pore volume:  $0.59\text{ cm}^3/\text{g}$ , pellet size: 40–60 mesh) was washed with hot deionized water 10 times. The loading of Co was 15 wt %.

**2.2. Catalytic Performance Testing.** The catalytic performance of the resulting Co– $\text{Co}_2\text{C}/\text{AC}$  catalyst for 1-hexene hydroformylation was tested in the same fixed-bed continuous-flow stainless microreactor as for the catalyst pretreatment (including the steps of drying, calcinations, reduction, and carburization). Also, the catalytic behavior of the Co– $\text{Co}_2\text{C}$  catalyst was tested in the fixed-bed continuous-flow stainless microreactor. The volume of catalyst was 2 mL for each test. The 1-hexene was fed into the catalyst bed at a liquid hourly space velocity (LHSV) of  $0.6\text{ h}^{-1}$  together with syngas ( $\text{H}_2/\text{CO} = 1:1$ , GHSV =  $500\text{ h}^{-1}$ ) at 3.0 MPa pressure. The effluent passed through a high-pressure gas–liquid separator in an ice–water bath to collect the liquid product. After the initial reaction time of 20 h, the liquid product in the separator was emptied, and then, the sample reacted for 24 h was taken for analysis. Thus, the total reaction time was 44 h. It was off-line analyzed on HP-6890N GC with FFAP columns and FID detector.

The textural properties of fresh and used catalysts were determined via  $\text{N}_2$  physisorption at 77 K, using a Micromeritics ASAP 2420 instrument. Each sample was degassed under a vacuum at 363 K for 1 h and 623 K for 8 h prior to the measurement. The pore size distribution and pore volume were determined by the BJH method, and the specific surface area was estimated by the BET method.

**2.3. Characterization.** The morphology and crystalline nature of the samples were studied by high-resolution transmission electronic microscopy (HRTEM) using a Tecnai G2 F30 S-Twin electron microscope, operating at 300 kV. A few droplets of a suspension of the postreaction catalysts in ethanol were put on a microgrid carbon polymer supported on a copper grid and allowed to dry at room temperature for HRTEM observations.

The crystalline phases of catalysts were examined by X-ray diffraction (XRD) with  $\text{Cu K}\alpha_1$  radiation on a PANalytical X'Pert PRO diffractometer at 40 kV and 40 mA. The spectra were recorded from 5 to  $70^\circ$  at a scanning rate of  $10^\circ/\text{min}$ . For the measurements, the catalysts were ground to fine powder and placed inside a dish.

The X-ray fluorescence (XRF) measurement was carried out using a Philips MagiX spectrometer to determine the cobalt content of the catalyst before and after 1-hexene hydroformylation. Inductively coupled plasma with atomic emission spectra (ICP-AES) analyses of reaction mixtures after the 1-hexene hydroformylation reaction were performed in a Perkin-Elmer 1200 instrument.

**2.4. Calculation Details.** All the spin-polarized calculations were carried out by using density functional theory (DFT) as

Table 1. Hydroformylation Performance of 1-Hexene over Co–Co<sub>2</sub>C/AC Catalysts at 453 K and 3.0 MPa<sup>a</sup>

carbonization time (h)	Co <sub>2</sub> C/Co (XRD intensity) <sup>b</sup>	1-hexene conv. (%)	hydroformylation selectivity (%)				hydrogenation sel. (%)	isomerization sel. (%)
			nal <sup>c</sup>	noI <sup>d</sup>	l/b <sup>e</sup>	total		
0	0.21	10.5	7.1	21.2	5.6	28.2	48.8	22.9
2	0.36	12.7	11.6	21.9	6.2	33.5	44.3	22.2
20	1.01	19.0	9.7	34.7	7.3	44.4	38.1	17.5
40	1.19	18.2	14.0	21.3	9.4	35.4	43.2	21.4
250	2.16	8.5	12.4	16.0	12.9	28.4	43.5	28.1

<sup>a</sup>Reaction conditions:  $T = 453$  K,  $P = 3.0$  MPa, GHSV of syngas ( $H_2/CO = 1$ ) =  $500$  h<sup>-1</sup>, LHSV of 1-hexene =  $0.6$  h<sup>-1</sup>. The data was taken for 24 h (the total reaction time was 44 h). The catalyst first reduced at 703 K and atmospheric pressure in a flow  $H_2$  ( $500$  h<sup>-1</sup>), then carburized at 493 K and 3.0 MPa in a flow of syngas ( $500$  h<sup>-1</sup>,  $H_2/CO = 1$ ) for (D) 0 h, (E) 2 h, (F) 20 h, (G) 40 h, and (H) 250 h. <sup>b</sup>The catalyst used after hydroformylation. <sup>c</sup>Heptanal. <sup>d</sup>Heptanol. <sup>e</sup>Linear/branched ratio.

implemented in the Vienna ab initio Simulation Package (VASP)<sup>27,28</sup> with the projector augmented wave (PAW) method.<sup>29</sup> We used the Perdew–Burke–Ernzerhof functional to evaluate the nonlocal exchange correlation energy.<sup>30</sup> In order to avoid the interaction between the two nearest neighbor slabs, the vacuum region between slabs was specified by 15 Å. The energy and force convergence were  $1 \times 10^{-4}$  and 0.02 eV, respectively.  $p(2 \times 1)$  unit cells for the Co<sub>2</sub>C (110) and (111) surfaces were utilized in our calculations, while  $p(1 \times 2)$  unit cells, for the Co<sub>2</sub>C (101) surface. A  $p(2 \times 2)$  unit cell was applied for the FCC Co (111) and stepped (311) surfaces. All the surfaces were simulated by containing four equivalent (111) Co layer slabs. The topmost two equivalent (111) Co layers including all C atoms are fully relaxed. Monkhorst–Packmesh<sup>31</sup>  $k$ -points of  $(6 \times 6 \times 1)$ ,  $(5 \times 5 \times 1)$ ,  $(4 \times 6 \times 1)$ ,  $(3 \times 6 \times 1)$ , and  $(6 \times 4 \times 1)$  were used for FCC Co (111) and (311) and Co<sub>2</sub>C (110), (111), and (101) surface calculations, respectively. The transition states (TS) were located by the force reversed method,<sup>32</sup> and a force tolerance of 0.02 eV/Å was utilized. We also searched the TSs of some of the minimum-energy reaction pathways by using the climbing image nudged elastic band (CI-NEB) method.<sup>33,34</sup> Here we considered both the C-terminated and C-terminated Co<sub>2</sub>C surfaces which correspond to Co rich and C rich conditions and are labeled as Co–Co<sub>2</sub>C and C–Co<sub>2</sub>C surfaces, respectively. The C–Co<sub>2</sub>C (101) surface has been reconstructed when CO, O, and H molecules or atoms adsorb on this surface.

The determined equilibrium lattice constants for bulk FCC Co and orthogonal Co<sub>2</sub>C are  $a = b = c = 3.520$  Å and  $a = 2.872$ ,  $b = 4.364$ , and  $c = 4.357$ , respectively.

### 3. RESULTS AND DISCUSSION

**3.1. Catalytic Performance.** Table 1 illustrates the catalytic performances of 1-hexene hydroformylation over Co–Co<sub>2</sub>C/AC catalyst prepared by tuning the carburization time (the carburization times were 0, 2, 20, 40, and 250 h, respectively) at 453 K and 3.0 MPa conditions. The main oxygenates derived from 1-hexene hydroformylation are *n*-heptanal, *i*-heptanal, *n*-heptanol, and *i*-heptanol. The by-products include hexane from hydrogenation and *i*-hexene (2-hexene and 3-hexene) from isomerization. It showed that the 1-hexene conversion and selectivities toward oxygenates on Co–Co<sub>2</sub>C/AC catalyst without being carburized (the carburization time was 0 h) were 10.5 and 28.2%, respectively. While the Co–Co<sub>2</sub>C/AC catalyst was synthesized with carburization for 2 h, the conversion of 1-hexene was increased slightly, while its selectivity toward heptanal and heptanol increased obviously with values of 11.6 and 21.9%, respectively. By increasing the carburization time to 20 h, the conversion of 1-hexene and

selectivity toward heptanal and heptanol on the Co–Co<sub>2</sub>C/AC catalyst increased dramatically up to 19.0 and 44.4%, respectively. However, the conversion of 1-hexene nearly remained unchanged and the selectivity toward heptanal and heptanol decreased slightly with the carburization time extending to 40 h. The Co–Co<sub>2</sub>C/AC catalyst carburized for 250 h showed low conversion of 1-hexene (8.5%) and selectivity toward heptanal and heptanol of 28.4%, and this catalytic performance is almost similar to that of the Co–Co<sub>2</sub>C/AC catalyst without being carburized. The results demonstrated that the 1-hexene conversion as well as selectivity to heptanal and heptanol over the Co–Co<sub>2</sub>C/AC catalysts depended on the carburization time of the catalyst dramatically. Meanwhile, the Co–Co<sub>2</sub>C/AC catalyst carburized for 20 h showed the highest catalytic activity and selectivity of 1-hexene hydroformylation.

On traditional supported cobalt-based heterogeneous catalysts for 1-hexene hydroformylation, such as Co/AC catalyst, the selectivity toward oxygenates (heptanal and heptanol) was about 85%, which was higher than that of our Co–Co<sub>2</sub>C/AC catalyst here.<sup>5</sup> For instance, for the Co/AC catalyst reported by Zhang and our Co–Co<sub>2</sub>C/AC catalyst without carburization, the preparation methods for the two catalysts were almost the same. Namely, both of the two catalysts were almost the same. However, the reaction conditions of the catalysts for hydroformylation of 1-hexene were obviously different from each other. Our catalytic test was carried out at 453 K and 3.0 MPa, while the catalytic test of the Co/AC reported by Zhang was carried out under the typical hydroformylation conditions of 403 K and 5.0 MPa. At low temperature, the hydrogenation rate of 1-hexene on the Co/AC catalyst is quite low. However, the hydrogenation rate of 1-hexene on the Co–Co<sub>2</sub>C/AC catalyst is relatively higher with the selectivity to 1-hexane of 48.8% at a high temperature of 453 K. Meanwhile, the selectivity toward aldehydes and alcohols is also somewhat inhibited. However, at the same high temperature of 453 K, the Co–Co<sub>2</sub>C/AC catalyst carburized for 20 h exhibited the higher selectivity toward oxygenates than that of the Co–Co<sub>2</sub>C/AC catalyst without carburization. It indicated that the traditional supported Co/AC catalyst might show poor activity and selectivity of hydroformylation of 1-hexene at 453 K.

To exclude the possible role of the supports, we have synthesized the unsupported bulk Co–Co<sub>2</sub>C catalysts and evaluated their catalytic performances of hydroformylation of 1-hexene. A Co<sub>3</sub>O<sub>4</sub> sample is first reduced under a condition of 703 K and atmospheric pressure in a flow of pure  $H_2$  (GHSV =  $500$  h<sup>-1</sup>) and then carburized at 493 K and 3.0 MPa in a flow of pure CO ( $500$  h<sup>-1</sup>) for 250 h to obtain the Co<sub>2</sub>C sample. As presented in Table 2, the Co<sub>2</sub>C catalyst showed a significantly

Table 2. Hydroformylation Performance of 1-Hexene over Co–Co<sub>2</sub>C Catalysts

catalysts	Co <sub>2</sub> C/Co (XRD intensity)		1-hexene conv. (%)	hydroformylation sel. (%)				hydrogenation sel. (%)	isomerization sel. (%)
	before reaction	after reaction		nal <sup>b</sup>	nol <sup>c</sup>	l/b <sup>d</sup>	total		
A <sup>a</sup>	7.50	5.90	2.1	8.1	2.8	2.6	10.9	32.2	56.9
B <sup>a</sup>	0.72	0.70	2.7	21.0	21.0	10.4	42.0	22.6	35.5
C <sup>a</sup>	0.15	0.27	2.3	7.2	13.7	8.2	20.9	42.1	37.0

<sup>a</sup>Reaction conditions:  $T = 453$  K,  $P = 3.0$  MPa, GHSV of syngas ( $H_2/CO = 1$ ) =  $500$  h<sup>-1</sup>, LHSV of 1-hexene =  $0.6$  h<sup>-1</sup>. The data was taken for 24 h (the total reaction time was 44 h). (A) The carburized sample; (B) the one-step-decomposed sample; (C) the two-step-decomposed sample. <sup>b</sup>Heptanal. <sup>c</sup>Heptanol. <sup>d</sup>Linear/branched ratio.

Table 3. Hydroformylation Performance of 1-Hexene over the Co–Co<sub>2</sub>C/AC Catalysts on 443 K<sup>a</sup>

carbonization time (h)	1-hexene conv. (%)	hydroformylation sel. (%)				hydrogenation sel. (%)	isomerization sel. (%)
		nal <sup>b</sup>	nol <sup>c</sup>	l/b <sup>d</sup>	total		
0	8.3	11.3	18.5	4.7	29.8	45.7	24.5
2	9.0	14.0	20.2	4.0	34.2	40.6	25.1
20	10.3	19.1	26.6	7.2	45.7	33.3	21.0
40	13.0	20.4	22.3	6.8	42.7	33.6	23.8
250	5.1	15.8	14.3	7.7	29.8	32.9	37.3

<sup>a</sup>Reaction conditions:  $T = 443$  K,  $P = 3.0$  MPa, GHSV of syngas ( $H_2/CO = 1$ ) =  $500$  h<sup>-1</sup>, LHSV of 1-hexene =  $0.6$  h<sup>-1</sup>. The data was taken for 24 h (the total reaction time was 44 h). The catalyst first reduced at 703 K and atmospheric pressure in a flow  $H_2$  ( $500$  h<sup>-1</sup>), then carburized at 493 K and 3.0 MPa in a flow of syngas ( $500$  h<sup>-1</sup>,  $H_2/CO = 1$ ) for (D) 0 h, (E) 2 h, (F) 20 h, (G) 40 h, and (H) 250 h. <sup>b</sup>Heptanal. <sup>c</sup>Heptanol. <sup>d</sup>Linear/branched ratio.

low 1-hexene conversion of 2.1% and low selectivity toward oxygenates of 10.9%, which were much lower than those of the supported Co–Co<sub>2</sub>C/AC catalyst. Interestingly, a high 1-hexene hydroformylation selectivity of 42.0% and a relative low selectivity toward olefin hydrogenation and carbon–carbon double bond isomerization are achieved for the one-step-decomposed Co–Co<sub>2</sub>C catalyst. The 1-hexene conversion over one-step-decomposed Co–Co<sub>2</sub>C catalyst increased slightly to 2.7%. For the two-step-decomposed Co–Co<sub>2</sub>C catalyst, the selectivity to oxygenate decreased down to 20.9%. Weller and Mohandas have reported that Co<sub>2</sub>C as prepared can be partially decomposed to the Co metal at higher temperature.<sup>17,20</sup> It could be concluded that the higher selectivity to oxygenate of the one- or two-step-decomposed Co–Co<sub>2</sub>C catalyst might originate from the mixed Co<sub>2</sub>C and metallic Co species.

By comparison with the supported Co–Co<sub>2</sub>C/AC catalysts, the unsupported bulk Co–Co<sub>2</sub>C catalysts showed low catalytic activity with the 1-hexene conversion of about 2%, which was properly due to their low dispersion degree of catalytic sites. The catalytic performances of 1-hexene hydroformylation over the bulk Co–Co<sub>2</sub>C catalysts can reach to a maximum by changing the decomposition pretreatment methods. For the one-step-decomposed Co–Co<sub>2</sub>C catalyst, the selectivity of oxygenates, including heptanal (selectivity of heptanal: 9.7%) and heptanol (selectivity of heptanol: 34.7%), was 44.4%. The Co–Co<sub>2</sub>C/AC catalyst carburized for 20 h showed the almost same selectivity of oxygenates (selectivity of heptanal: 21.0%; selectivity of heptanol: 21.0%) as 42%. The catalytic behavior over the Co–Co<sub>2</sub>C catalysts by changing the decomposition pretreatment methods was similar to that of the supported Co–Co<sub>2</sub>C/AC catalysts by tuning the carburization time.

**3.2. The Influence of the Reaction Temperature and Pressure over Co–Co<sub>2</sub>C/AC Catalyst.** In this part, we have investigated the effect of reaction temperature and pressure on 1-hexene conversion and selectivities of the products. The catalytic performances of 1-hexene hydroformylation at 443 K over the Co–Co<sub>2</sub>C/AC catalysts prepared by tuning the carburization time (the carburization times were 0, 2, 20, 40,

and 250 h, respectively) were shown in Table 3. It was found that the 1-hexene conversion decreased from 19.0 to 10.3% when the reaction temperature decreased from 453 to 443 K and the hydroformylation selectivity almost stayed the same over the Co–Co<sub>2</sub>C/AC catalyst with a carburization time of 20 h. For the other Co–Co<sub>2</sub>C/AC catalyst prepared with various carburization times, the lower 1-hexene conversion was also observed at a reaction temperature of 443 K. By comparison with the data in Tables 1 and 3, we found that the reaction temperature has a considerable impact on the reaction rates of 1-hexene hydroformylation.

The effect of reaction pressure on the performance of 1-hexene hydroformylation of the Co–Co<sub>2</sub>C/AC with a carburization time of 20 h is demonstrated in Figure 1. Interestingly, the optimized reaction pressure is 3.0 MPa, under which conditions both the 1-hexene conversion and hydroformylation selectivity reach to a maximum, even though the differences among various reaction pressures are very small. This result was different from that of the traditional supported

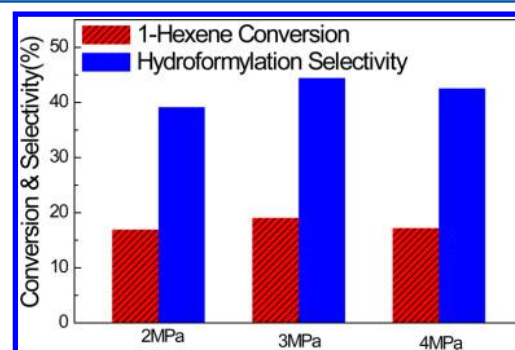


**Figure 1.** Effect of pressure on the performance of 1-hexene hydroformylation over the Co–Co<sub>2</sub>C/AC catalyst carburized for 20 h. Reaction conditions:  $T = 453$  K, GHSV of syngas ( $H_2/CO = 1$ ) =  $500$  h<sup>-1</sup>, LHSV of 1-hexene =  $0.6$  h<sup>-1</sup>. The data was taken for 24 h (the total reaction time was 44 h).

cobalt-based catalyst, on which the conversion of 1-hexene and selectivity toward oxygenates increased with the reaction pressure. It implied that the catalytic reaction mechanism of the Co–Co<sub>2</sub>C/AC for 1-hexene hydroformylation was distinct from that of the supported cobalt-based catalyst.<sup>7</sup>

**3.3. The Stability of Co–Co<sub>2</sub>C/AC Catalyst.** The stability of 1-hexene hydroformylation selectivity and conversion with time on stream are illustrated in Figure 2. It is obvious that an

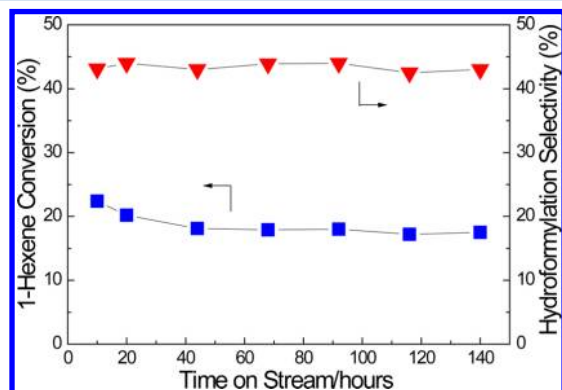


**Figure 2.** Stability of 1-hexene conversion and hydroformylation selectivity with time on stream over the Co–Co<sub>2</sub>C/AC catalyst carburized for 20 h. Reaction conditions:  $T = 453$  K, GHSV of syngas ( $H_2/CO = 1$ ) =  $500$  h<sup>-1</sup>, LHSV of 1-hexene =  $0.6$  h<sup>-1</sup>, reaction time = 140 h.

initial activity is observed before 40 h time on stream, and then, 1-hexene conversion keeps constant for a long-term continuous reaction. During the reaction time, the hydroformylation selectivity always sustains at ca. 43%. From Table 4, we can

**Table 4. Co Content in the Co–Co<sub>2</sub>C/AC Catalyst Carburized for 20 h before and after Hydroformylation Reaction of 1-Hexene for 140 h**

catalyst	Co content (wt %)	
	fresh	used
Co–Co <sub>2</sub> C/AC	13.1 <sup>a</sup>	13.3 <sup>a</sup>
	12.7 <sup>b</sup>	12.3 <sup>b</sup>

<sup>a</sup>Detected by XRF measurement. <sup>b</sup>Detected by ICP-AES measurement. Reaction conditions:  $T = 453$  K,  $P = 3.0$  MPa, GHSV of syngas ( $H_2/CO = 1$ ) =  $500$  h<sup>-1</sup>, LHSV of 1-hexene =  $0.6$  h<sup>-1</sup>, reaction time = 140 h.

see that the Co content of 12.7% in the fresh Co–Co<sub>2</sub>C/AC catalyst and that of 12.3% in the spent one after more than 140 h reaction time were detected by AEM-ICP techniques, indicating that no soluble cobalt carbonyl species were formed and thus led to no cobalt elution during hydroformylation under reaction conditions. Our experimental results are consistent with previous findings that the formation of cobalt carbonyls is hindered under reaction temperatures higher than 443 K and reaction pressures lower than 3.0 MPa.<sup>35</sup> Our Co–Co<sub>2</sub>C/AC catalysts are tested at a higher temperature of 453 K, which might be responsible for the high stability of 1-hexene hydroformylation compared to the supported cobalt-based catalyst reported in the literature.<sup>5–8</sup> In addition, the high stability might also be correlated with the pretreatments of our Co–Co<sub>2</sub>C/AC sample which were executed in a flow of syngas ( $H_2/CO = 1$ ,  $500$  h<sup>-1</sup>) under 493 K and 3.0 MPa to form the mixed Co<sub>2</sub>C and metallic Co species.

**3.4. Characterization.** Figure 3 shows the XRD patterns of the spent Co–Co<sub>2</sub>C/AC catalysts carburized for different times

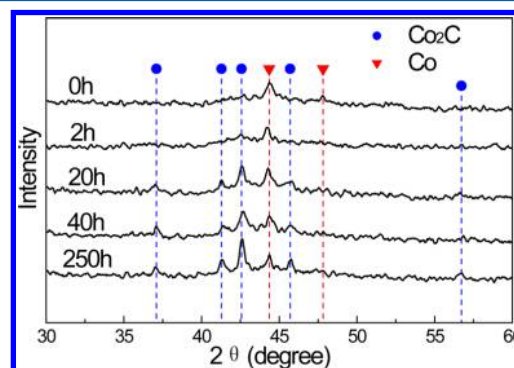


**Figure 3.** XRD pattern of the spent Co–Co<sub>2</sub>C/AC catalysts carburized for different times after 1-hexene hydroformylation reaction at 453 K and 3.0 MPa.

after 1-hexene hydroformylation reaction at 453 K and 3.0 MPa for 44 h. The apparent diffraction peaks at  $2\theta = 44.3$  and  $47.5^\circ$ , which were found on the Co–Co<sub>2</sub>C/AC catalyst used without carburization after hydroformylation, were ascribed to the metallic Co species. When the sample was prepared with carburization for 2 h, the observed new peaks at  $2\theta = 37.0$ ,  $41.3$ ,  $42.5$ ,  $45.7$ , and  $56.6^\circ$  can be attributed to the highly dispersed Co<sub>2</sub>C species. The intensities of the diffraction peaks for Co<sub>2</sub>C increased with the carburization time, in contrast with the intensities of the peaks for metallic Co that decreased with the increase of carburization time. The longer the carburization time, the stronger the diffraction peaks for Co<sub>2</sub>C. These results indicated that the Co<sub>2</sub>C could be formed in a way that metallic Co was carburized at 493 K and 3.0 MPa in a syngas flow ( $H_2/CO = 1:1$ , GHSV =  $500$  h<sup>-1</sup>). X-ray diffraction intensity ratios of Co<sub>2</sub>C to Co are listed in Table 1. Interestingly, the catalytic performances of the 1-hexene hydroformylation on the Co–Co<sub>2</sub>C/AC catalysts were obviously related to the X-ray diffraction intensity ratios of Co<sub>2</sub>C to Co (Co<sub>2</sub>C/Co). When the X-ray diffraction intensity ratios of Co<sub>2</sub>C to Co were too high or too low, the catalytic activity and selectivity of the 1-hexene hydroformylation were poor. However, when the X-ray diffraction intensity ratios (Co<sub>2</sub>C/Co) are moderate, such as 1, meaning that the catalyst contained nearly equivalent Co<sub>2</sub>C species and metallic species, the highest conversion rate of olefins and selectivity of hydroformylation were achieved.

In order to identify the origin of the higher activity of Co–Co<sub>2</sub>C/AC catalyst for 1-hexene hydroformylation, HRTEM has been used to characterize the active sites. Figure 4 shows the HRTEM images of the Co–Co<sub>2</sub>C/AC catalyst carburized for 20 h after 1-hexene hydroformylation. The clean lattice fringe of 4.18 and 1.63 Å as well as the angle of  $53.7^\circ$  between two lattice fringes are the characteristic interlayer spacing of the Co-fcc(110) and Co-fcc(125) planes and their corresponding angle. The good crystallinity of Co<sub>2</sub>C can be justified from the lattice fringe of 2.13 and 1.61 Å as well as the angle of  $80.8^\circ$  between them, corresponding to Co<sub>2</sub>C(111) and Co<sub>2</sub>C(–121) planes. Co<sub>2</sub>C and Co are always coexisting in Co–Co<sub>2</sub>C/AC catalyst carburized for 20 h. The Co–Co<sub>2</sub>C/AC catalysts containing predominantly Co<sub>2</sub>C or Co will have lower activity and selectivity for 1-hexene hydroformylation. Therefore, we derived that the interfacial active sites between Co species and Co<sub>2</sub>C species in Co–Co<sub>2</sub>C/AC catalysts might be responsible

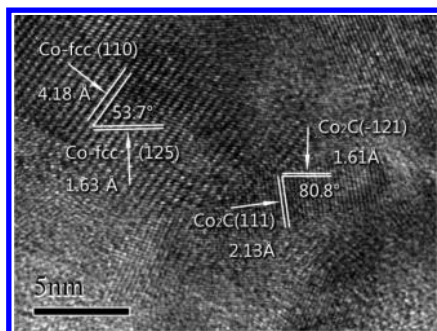


**Figure 4.** HRTEM images of the Co–Co<sub>2</sub>C/AC catalyst used carburized for 20 h after 1-hexene hydroformylation reaction. Reaction conditions:  $T = 453$  K,  $P = 3.0$  MPa, GHSV of syngas ( $H_2/CO = 1$ ) =  $500$  h<sup>-1</sup>, LHSV of 1-hexene =  $0.6$  h<sup>-1</sup>.

for hydroformylation of olefins. On the basis of the above observations, it can be concluded that the active sites for olefin hydroformylation on the Co–Co<sub>2</sub>C/AC catalyst are different from those of the Co/AC catalyst reported in the literature.

To see the support effect, we have also studied the Co–Co<sub>2</sub>C catalytic system. XRD patterns of the carburized sample, i.e., the one-step-decomposed sample in a flow of H<sub>2</sub> ( $500$  h<sup>-1</sup>) for 20 h at 523 K and the two-step-decomposed sample in a flow of H<sub>2</sub> ( $500$  h<sup>-1</sup>) for 20 h at 523 K and further at 543 K, are shown in Figure 5. The only apparent diffraction peaks at  $2\theta = 37.0$ ,  $41.3$ ,  $42.5$ ,  $45.7$ , and  $56.6^\circ$  were observed on the carburized sample and could be attributed to the lowly dispersed Co<sub>2</sub>C species. However, the weak peaks at  $2\theta = 42.7$ ,  $44.3$ , and  $47.5^\circ$  detected on the used carburized sample after hydroformylation were attributed to the metallic Co species, suggesting that a little of the Co<sub>2</sub>C species was decomposed into metallic Co species under the 1-hexene hydroformylation conditions:  $T = 453$  K,  $P = 3.0$  MPa, GHSV of syngas ( $H_2/CO = 1:1$ ) =  $500$  h<sup>-1</sup> and LHSV of 1-hexene =  $0.6$  h<sup>-1</sup> for 44 h. A mixture of Co<sup>0</sup> and Co<sub>2</sub>C species is found in both the one-step-decomposed and two-step-decomposed samples before hydroformylation, while the X-ray diffraction intensity ratio of Co<sub>2</sub>C/Co in the former sample (0.72) is significantly higher than that in the latter (0.15), as shown in Table 2. It suggested that the Co<sub>2</sub>C species was decomposed into metallic Co at 523 K in a flow of H<sub>2</sub>, and the decomposition degree of the Co<sub>2</sub>C is enhanced with the increase of decomposition temperature.

The good crystallinity of Co<sub>2</sub>C in the carburized sample is further confirmed by HRTEM measurements, as shown in

Figure 6a. The lattice fringe of 2.45 and 2.46 Å as well as the angle of  $64.5^\circ$  between the two lattice fringes are the interlayer spacing of Co<sub>2</sub>C (–110) and (110) planes and the corresponding angle, and another lattice fringe of 2.19 Å can be ascribed to the Co<sub>2</sub>C (020) plane. In the one-step-decomposed sample, not only the Co<sup>0</sup>-fcc{111} lattice fringe is detected, but also the Co<sub>2</sub>C (101) and (001) planes are observed (Figure 6b). Interestingly, the HRTEM image in Figure 6c shows a typical Co<sup>0</sup>-hcp (–114) and (023) and Co<sub>2</sub>C (10–1) and (101) planes detected in the spent carburized sample after hydroformylation reaction. The prominent Co<sup>0</sup>-fcc{111} and Co<sub>2</sub>C (002) and (110) lattice fringes are also found in the spent one-step-decomposed sample after hydroformylation, as shown in Figure 6d.

Combined with the catalytic performances on the Co–Co<sub>2</sub>C catalysts, the ratio of the X-ray diffraction intensities of Co<sub>2</sub>C/Co being 0.72 was more favorable for the 1-hexene hydroformylation reaction. This result further confirmed the above findings that the Co<sub>2</sub>C–Co/AC catalyst has the largest 1-hexene hydroformylation activity when the X-ray diffraction intensity ratio of Co<sub>2</sub>C/Co is 1. Moreover, the possible role of activated carbon support of the Co–Co<sub>2</sub>C/AC catalyst was excluded through such research on Co–Co<sub>2</sub>C catalyst. Therefore, it is reasonable to conclude that the interfacial active sites between Co and Co<sub>2</sub>C are responsible for the high activity and selectivity for 1-hexene hydroformylation reaction.

**3.5. DFT Calculations.** To provide a mechanistic understanding of 1-hexene hydroformylation reaction on the Co–Co<sub>2</sub>C and Co–Co<sub>2</sub>C/AC catalysts, CO adsorption and activation on the experimentally observed Co<sub>2</sub>C (101) surface, including Co-terminated and C-terminated surfaces (see Figure 7), and the stepped Co (311) surface which is reported to be highly active for CO activation,<sup>36,37</sup> has been investigated first by DFT calculations. The calculated CO activation potential energy surface and details are given in Figure S2 and Table S1–S4 (Supporting Information). It is obvious that CO prefers to adsorb molecularly on the Co-terminated Co<sub>2</sub>C (101) surface at the 3-fold site (Figure 7) with an adsorption energy of  $-2.02$  eV, which is stronger than that of the stepped Co (311) surface by 0.31 eV. The data in Figure S2 (Supporting Information) shows that CO dissociation is difficult on the Co-terminated Co<sub>2</sub>C (101) surface by either the direct dissociation route with a large activation barrier of 1.56 eV or the H-assisted CO dissociation route with an overall barrier of 1.64 eV. Though the CO adsorption energy of  $-1.69$  eV on the C-terminated Co<sub>2</sub>C (101) surface is almost the same as that on the stepped

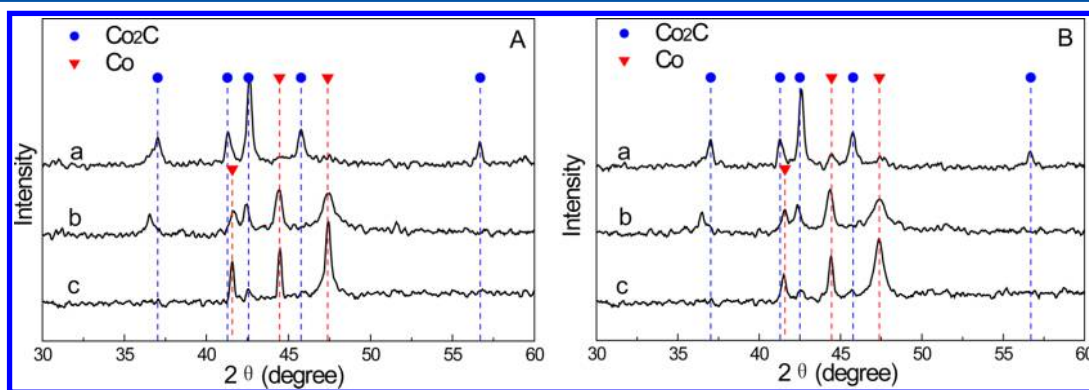


**Figure 5.** XRD patterns of samples before hydroformylation (A) and after hydroformylation (B): (a) the carburized sample; (b) the one-step-decomposed sample; (c) the two-step-decomposed sample.

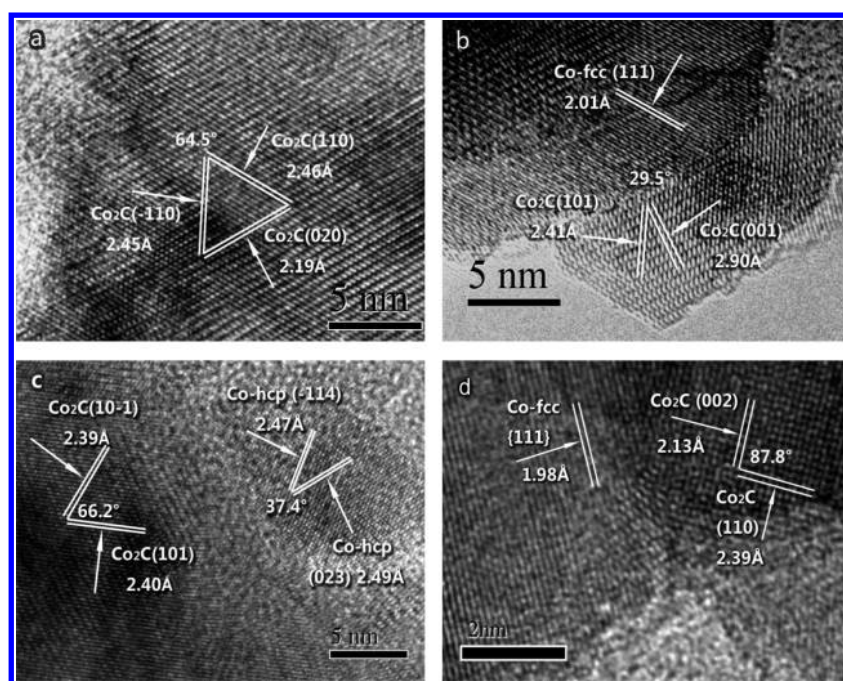


**Figure 6.** HRTEM images of the  $\text{Co}_2\text{C}$  and  $\text{Co-Co}_2\text{C}$  samples: (a) the carburized sample before hydroformylation; (b) the one-step-decomposed sample before hydroformylation; (c) the carburized sample after hydroformylation; (d) the one-step-decomposed sample after hydroformylation.

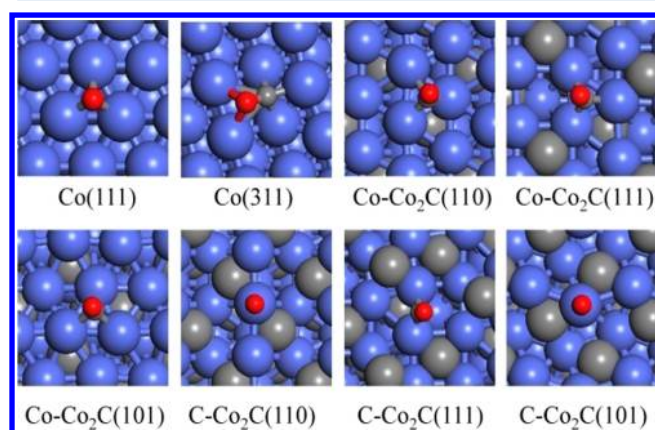


**Figure 7.** Configurations for the adsorption of CO molecule on FCC Co (111), stepped (311), Co-terminated, and C-terminated  $\text{Co}_2\text{C}$  (110), (111), and (101) surfaces (blue, Co atom; gray, C atom; red, O atom; white, H atom, same as follows).

Co (311) surface ( $-1.71$  eV), the CO activation barrier is still  $2.04$  eV high considering the two CO activation pathways. Meanwhile, our previous calculations have revealed that CO activation barriers on the Co-terminated and C-terminated  $\text{Co}_2\text{C}$  (110) and the  $\text{Co}_2\text{C}$  (111) surfaces are at least  $1.86$  eV, which is also forbiddingly large to be a dominant pathway for breaking of the  $\text{C}=\text{O}$  bond. The data shown in Table 5 illustrates that the CO binding strength on the  $\text{Co}_2\text{C}$  (110) and (111) surfaces would be at least  $0.30$  and  $0.15$  eV, respectively, stronger than that on the stepped Co (311) surface. The stronger adsorption of CO on  $\text{Co}_2\text{C}$  surfaces can be ascribed to the combination of the lattice expansion, and enhanced  $5\sigma$  donation owing to the positive charge of the topmost surface cobalt.<sup>38,39</sup> Our DFT calculations show that CO prefers to molecularly adsorb on the Co-terminated or C-terminated  $\text{Co}_2\text{C}$  surface without dissociation under low temperatures ( $T = 443\text{--}453$  K), with a larger bonding strength on the  $\text{Co}_2\text{C}$

**Table 5.** Adsorption Energy (in eV) and Favorable Adsorption Sites of CO and Ethylene ( $\text{C}_2\text{H}_4$ ) on Co-Terminated and C-Terminated  $\text{Co}_2\text{C}$  (110), (111), and (101) and FCC Co (111) and (311) Surfaces<sup>a</sup>

surface	$E_{\text{CO}}$	geometry	$E_{\text{C}_2\text{H}_4}$	geometry
FCC Co (111)	$-1.61$	HCP	$-0.60$	C-hcp-C-top
FCC Co (311)	$-1.71$	edge-FCC	$-1.05$	C-bridge-C-top
Co- $\text{Co}_2\text{C}$ (110)	$-2.01$	3-site	$-1.25$	C-bridge-C-top
Co- $\text{Co}_2\text{C}$ (111)	$-2.21$	3-site	$-1.19$	C-hollow-C-top
Co- $\text{Co}_2\text{C}$ (101)	$-2.02$	3-site	$-1.44$	C-bridge-C-top
C- $\text{Co}_2\text{C}$ (110)	$-2.11$	top	$-1.56$	C-bridge-C-top
C- $\text{Co}_2\text{C}$ (111)	$-1.86$	bridge	$-1.31$	C-bridge-C-top
C- $\text{Co}_2\text{C}$ (101)	$-1.69$	top	$-0.90$	C-top-C-top

<sup>a</sup>The adsorption energies are calculated with respect to the corresponding molecules in the gas phase.

(101), (110), and (111) surfaces than on the stepped Co (311) surface.

The alkene adsorption on the  $\text{Co}_2\text{C}$  and the stepped Co surfaces has also been studied. For simplification, ethylene is used as a probe olefin molecule and the calculation results are given in Table 5 and Figure 8. It is found that ethylene adsorbs at the topmost Co atom of the stepped Co (311) with an adsorption energy of  $-1.05$  eV, and the ethylene binding strength is  $0.45$  eV stronger than that of the flat Co (111) surface. The calculated ethylene adsorption energies on the  $\text{Co}_2\text{C}$  (110) and (111) and the Co-terminated  $\text{Co}_2\text{C}$  (101) surfaces fall in the range of  $-1.19$  to  $-1.56$  eV, which are at least  $0.14$  eV larger than that on the stepped Co (311) surface. To clarify the influence of carbon number in alkenes, we have also studied the adsorption of propylene ( $\text{C}_3\text{H}_6$ ) on Co (311) and Co-terminated  $\text{Co}_2\text{C}$  (101) and (110) surfaces. The most favorable adsorption configurations of propylene on Co and  $\text{Co}_2\text{C}$  surfaces and their adsorption energies are shown in Figure S5 (Supporting Information). It is found that propylene has a weaker adsorption than ethylene on Co and  $\text{Co}_2\text{C}$

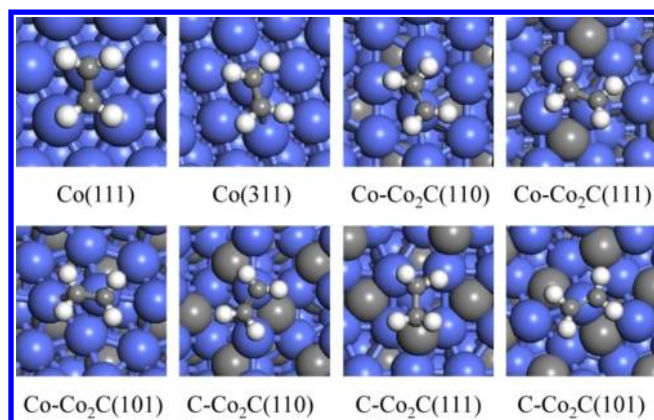


**Figure 8.** Configurations for the adsorption of ethylene molecule on FCC Co (111), stepped (311), Co-terminated, and C-terminated  $\text{Co}_2\text{C}$  (110), (111), and (101) surfaces.

surfaces. Like ethylene adsorption on  $\text{Co}_2\text{C}$  (101) and (110) surfaces, propylene adsorbs stronger than that of the Co (311) surface by 0.41 and 0.23 eV. Nevertheless, propylene adsorbs not so strongly as CO on  $\text{Co}_2\text{C}$  surfaces. Alkene adsorption on the metallic Co and  $\text{Co}_2\text{C}$  surfaces can be described by the DCD model with a donation of ethylene  $\pi$ -electrons into the metal and back-donation from the metal into the alkene antibonding  $\pi^*$  orbital.<sup>40,41</sup> A surface Co atom in the  $\text{Co}_2\text{C}$  surface has a positive charge, which is favorable for the  $\pi$ -electron donation into the metal and thus enhances alkene adsorption on the  $\text{Co}_2\text{C}$  surfaces.<sup>42</sup> This suggests that the olefin molecule is highly activated and C=C can migrate easily on the  $\text{Co}_2\text{C}$  compared to the Co surfaces. The present calculation results are consistent with the experimental findings that the selectivity for isomerization reaction is as high as 37.3% on the catalyst with a  $\text{Co}_2\text{C}/\text{Co}$  X-ray diffraction intensity ratio of 2.16 while lower (22.9%) on the catalyst with a majority of metallic Co (the X-ray diffraction intensity ratio of  $\text{Co}_2\text{C}/\text{Co}$  is 0.21).

When the X-ray diffraction intensity ratio of  $\text{Co}_2\text{C}/\text{Co}$  is 1, the Co- $\text{Co}_2\text{C}$  and Co- $\text{Co}_2\text{C}/\text{AC}$  catalysts will approach to a maximum of the interfacial active sites, where the highest conversion rate of olefins should be achieved. Either increase of the content of  $\text{Co}_2\text{C}$  or Co will lower the activity for the Co- $\text{Co}_2\text{C}$  and Co- $\text{Co}_2\text{C}/\text{AC}$  catalysts. On the Co- $\text{Co}_2\text{C}$  or Co- $\text{Co}_2\text{C}/\text{AC}$  catalysts containing predominantly  $\text{Co}_2\text{C}$ , a great number of CO prefers to strongly adsorb on  $\text{Co}_2\text{C}$  surfaces molecularly and leaves less active sites for olefin adsorption. The adsorption competition between CO and olefin leads to the low activity for 1-hexene hydroformylation. While on the Co- $\text{Co}_2\text{C}$  and Co- $\text{Co}_2\text{C}/\text{AC}$  catalysts with most metallic Co, the CO binding strength on Co surfaces is weaker than that on the  $\text{Co}_2\text{C}$  surfaces; the number of molecularly adsorbed and activated CO is thus less on the metallic Co sites, which also makes the catalysts have low 1-hexene hydroformylation activity. When there are more interfacial active sites between the metallic Co and  $\text{Co}_2\text{C}$  species, even more adsorbed CO on the  $\text{Co}_2\text{C}$  sites will insert into the abundant adsorbed olefin molecules on the metallic Co species, which increases olefin hydroformylation activity.

#### 4. CONCLUSIONS

Non-noble metals based on Co- $\text{Co}_2\text{C}$  and Co- $\text{Co}_2\text{C}/\text{AC}$  catalysts have been shown to be quite active and selective for 1-hexene hydroformylation under low pressure conditions. The

presence of the Co and  $\text{Co}_2\text{C}$  interfacial active sites is essential for the production of the oxygenates. The 1-hexene conversion as well as selectivity to heptanal and heptanol on the Co- $\text{Co}_2\text{C}/\text{AC}$  and Co- $\text{Co}_2\text{C}$  catalysts vary dramatically with the ratio of  $\text{Co}_2\text{C}/\text{Co}$  XRD intensity. The Co- $\text{Co}_2\text{C}/\text{AC}$  catalyst with the optimum ratio (1.01) of  $\text{Co}_2\text{C}/\text{Co}$  was obtained by carburizing the reduced metallic Co species of the Co/AC catalyst in a syngas flow ( $\text{H}_2/\text{CO} = 1:1$ , GHSV =  $500 \text{ h}^{-1}$ ) at 3.0 MPa and 493 K for 20 h. This Co- $\text{Co}_2\text{C}/\text{AC}$  catalyst showed higher catalytic activity and selectivity of 1-hexene hydroformylation in the fixed-bed continuous-flow reactor. It also exhibited good catalytic stability at 453 K and 3.0 MPa with a time on stream of 140 h without any cobalt elution, indicating that no cobalt dissolved carbonyl species formed and led to no cobalt elusion during hydroformylation under reaction conditions. Combined with the experimental results and theory study, it could be concluded that the high oxygenate selectivity originated from the synergetic effect; namely, Co species are used for the adsorption and activation of olefin to form the adsorbed surface carbonaceous species and the  $\text{Co}_2\text{C}$  species for CO molecular adsorption, activation, and insertion. When the ratio of  $\text{Co}_2\text{C}/\text{Co}$  XRD intensity was in the range 0.7–1.2, it meant that the content of  $\text{Co}_2\text{C}$  species is nearly equivalent to that of Co species and thus the interfacial active sites reach the maximum. As a result, higher catalytic performances of 1-hexene hydroformylation were achieved on the Co- $\text{Co}_2\text{C}$  and Co- $\text{Co}_2\text{C}/\text{AC}$  catalysts.

Our results have shown that the catalytic activity for 1-hexene hydroformylation of the catalyst containing metallic Co and  $\text{Co}_2\text{C}$  species could be improved by being loaded on the support. It could be speculated that the catalytic activity as well as selectivity of 1-hexene hydroformylation of the supported Co- $\text{Co}_2\text{C}$  catalysts might be further improved by employing some methods of catalyst preparation, such as by controlling the particle sizes of Co and  $\text{Co}_2\text{C}$  species, changing the support or adding the promoters, etc.

#### ■ ASSOCIATED CONTENT

##### Supporting Information

DFT calculation results of CO absorption and dissociation on different Co and  $\text{Co}_2\text{C}$  surfaces, along with alkene absorption. This material is available free of charge via the Internet at <http://pubs.acs.org>.

#### ■ AUTHOR INFORMATION

##### Corresponding Authors

\*E-mail: dyj@dicp.ac.cn. Phone: +86-411-84379143.

\*E-mail: wxli@dicp.ac.cn. Phone: +86-411-84379996.

##### Author Contributions

<sup>||</sup>W.D., J.L.: These authors contributed equally.

##### Notes

The authors declare no competing financial interest.

#### ■ ACKNOWLEDGMENTS

This work was supported by the National Natural Science Foundation of China (20973167, 21273224, and 21225315) and 973 Project (2013CB933100)

#### ■ REFERENCES

(1) Franke, R.; Selent, D.; Börner, A. Applied Hydroformylation. *Chem. Rev.* **2012**, *112*, 5675–5732.

- (2) Ungvary, F. Application of Transition Metals in Hydroformylation: Annual Survey Covering the Year 2006. *Coord. Chem. Rev.* **2007**, *251*, 2087–2102.
- (3) Lenarda, M.; Storaro, L.; Ganzerla, R. Hydroformylation of Simple Olefins Catalyzed by Metals and Clusters Supported on Unfunctionalized Inorganic Carriers. *J. Mol. Catal. A: Chem.* **1996**, *111*, 203–237.
- (4) Qiu, X.; Tsubaki, N.; Sun, S.; Fujimoto, K. Promoting Effect of Noble Metals to Co/SiO<sub>2</sub> Catalysts for Hydroformylation of 1-Hexene. *Catal. Commun.* **2001**, *2*, 75–80.
- (5) Zhang, Y.; Nagasaka, K.; Qiu, X.; Tsubaki, N. Low-Pressure Hydroformylation of 1-Hexene over Active Carbon-Supported Noble Metal Catalysts. *Appl. Catal., A* **2004**, *276*, 103–111.
- (6) Zhang, Y.; Shinoda, M.; Shiki, Y.; Tsubaki, N. Hydroformylation of 1-Hexene for Oxygenate Fuels via Promoted Cobalt/Active Carbon Catalysts at Low-Pressure. *Fuel* **2006**, *85*, 1194–1200.
- (7) Zhang, Y.; Nagasaka, K.; Qiu, X.; Tsubaki, N. Hydroformylation of 1-Hexene for Oxygenate Fuels on Supported Cobalt Catalysts. *Catal. Today* **2005**, *104*, 48–54.
- (8) Alvila, L.; Pursiainen, J.; Kiviaho, J.; Pakkanen, T. A.; Krause, O. Ru<sub>3</sub>(Co)<sub>12</sub>/2,2'-Bipyridine Supported on Inorganic Carriers as 1-Hexene Hydroformylation Catalysts. *J. Mol. Catal.* **1994**, *91*, 335–342.
- (9) Kainulainen, T. A.; Niemelac, M. K.; Krause, A. O. I. Hydroformylation of 1-hexene on Rh/C and Co/SiO<sub>2</sub> Catalysts. *J. Mol. Catal. A: Chem.* **1997**, *122*, 39–49.
- (10) Oyama, S. T. Preparation and Catalytic Properties of Transition-Metal Carbides and Nitrides. *Catal. Today* **1992**, *15*, 179–200.
- (11) Zheng, W. Q.; Cotter, T. P.; Kaghazchi, P.; Jacob, T.; Frank, B.; Schlichte, K.; Zhang, W.; Su, D. S.; Schuth, F.; Robert, S. Experimental and Theoretical Investigation of Molybdenum Carbide and Nitride as Catalysts for Ammonia Decomposition. *J. Am. Chem. Soc.* **2013**, *135*, 3458–3464.
- (12) Rodriguez, J. A.; Dvorak, J.; Jirsak, T. Chemistry of SO<sub>2</sub>, H<sub>2</sub>S, and CH<sub>3</sub>SH on Carbide-Modified Mo(110) and Mo<sub>2</sub>C Powders: Photoemission and XANES Studies. *J. Phys. Chem. B* **2000**, *104*, 11515–11521.
- (13) Yu, C. C.; Ramanathan, S.; Sherif, F.; Oyama, S. T. Structural, Surface, and Catalytic Properties of A New Bimetallic V-Mo Oxynitride Catalyst for Hydrodenitrogenation. *J. Phys. Chem.* **1994**, *98*, 13038–13041.
- (14) Nagai, M.; Zahidul, A. M.; Matsuda, K. Nano-Structured Nickel-Molybdenum Carbide Catalyst for Low-Temperature Water-Gas Shift Reaction. *Appl. Catal., A* **2006**, *313*, 137–145.
- (15) Keller, V.; Weher, P.; Garin, F.; Ducros, R.; Maire, G. Catalytic Activity Of Bulk Tungsten Carbides for Alkane Reforming 0.1. Characterization and Catalytic Activity for Reforming of Hexane Isomers in the Absence of Oxygen. *J. Catal.* **1995**, *15*, 9–16.
- (16) Ducreux, O.; Lynch, J.; Rebours, B.; Roy, M.; Chaumette, P. In Situ Characterisation of Cobalt Based Fischer–Tropsch Catalysts: A New Approach to the Active Phase. *Stud. Surf. Sci. Catal.* **1998**, *119*, 125–130.
- (17) Weller, S. L.; Hofer, J. E.; Anderson, R. B. The Role of Bulk Cobalt Carbide in The Fischer–Tropsch Synthesis. *J. Am. Chem. Soc.* **1948**, *70*, 799–801.
- (18) Bian, G.; Nanba, T.; Koizumi, N.; Yamada, M. Changes in Microstructure of A Reduced Cobalt Catalyst During Performing FT Synthesis From Syngas Determined by in Situ High-Pressure Syngas Adsorption. *J. Mol. Catal. A: Chem.* **2002**, *178*, 219–228.
- (19) Cheng, Jun.; Hu, P.; Ellis, Peter.; French, Sam.; Kelly, Gordon.; Lok, C. Martin. Density Functional Theory Study of Iron and Cobalt Carbides for Fischer–Tropsch Synthesis. *J. Phys. Chem. C* **2010**, *114*, 1085–1093.
- (20) Mohandas, J. C.; Gnanamani, M. K.; Jacobs, G.; Ma, W. P.; Ji, Y. Y.; Khalid, S.; Davis, B. H. Fischer–Tropsch Synthesis: Characterization and Reaction Testing of Cobalt Carbide. *ACS Catal.* **2011**, *1*, 1581–1588.
- (21) Volkova, G. G.; Yuriva, T. M.; Plyasova, L. M.; Naumova, M. I.; Zaikovskii, V. I. Role Of The Cu-Co Alloy and Cobalt Carbide in Higher Alcohol Synthesis. *J. Mol. Catal. A: Chem.* **2000**, *158*, 389–393.
- (22) Ding, Y. J.; Zhu, H. J.; Wang, T.; Jiao, G. P.; Lu, Y. US Patent 7,468,396, 2008, to Dalian Institute of Chemical Physics.
- (23) Ding, Y. J.; Zhu, H. J.; Wang, T.; Jiao, G. P.; Lu, Y. US Patent 7,670,985, 2010, to Dalian Institute of Chemical Physics.
- (24) Jiao, G. P.; Ding, Y. J.; Zhu, H. J.; Li, X. M.; Li, J. W.; Lin, R. H.; Dong, W. D.; Gong, L. F.; Pei, Y. P.; Lu, Y. Effect Of La<sub>2</sub>O<sub>3</sub> Doping on Syntheses of C<sub>–1</sub>–C<sub>–18</sub> Mixed Linear Alpha-Alcohols from Syngas over the Co/AC Catalysts. *Appl. Catal., A* **2009**, *364*, 137–142.
- (25) Pei, Y. P.; Ding, Y. J.; Zang, J.; Song, X. G.; Dong, W. D.; Zhu, H. J.; Wang, T.; Chen, W. M. Effects of Li Promoter on the Performance of Co/AC Catalysts for CO Hydrogenation to Mixed Linear alpha-Alcohols. *Chin. J. Catal.* **2012**, *33*, 808–812.
- (26) Lebarbier, V. M.; Mei, D. H.; Kim, D. H.; Andersen, A.; Male, J. L.; Holladay, J. E.; Rousseau, R.; Wang, Y. Effects of La<sub>2</sub>O<sub>3</sub> on the Mixed Higher Alcohols Synthesis from Syngas over Co Catalysts: A Combined Theoretical and Experimental Study. *J. Phys. Chem. C* **2011**, *115*, 17440–17451.
- (27) Kresse, G.; Hafner, J. Abinitio Molecular-Dynamics for Liquid-Metals. *Phys. Rev. B* **1993**, *47*, 558–561.
- (28) Kresse, G.; Furthmüller, J. Efficient Iterative Schemes for Ab Initio Total-Energy Calculations Using A Plane-Wave Basis Set. *Phys. Rev. B* **1996**, *54*, 11169–11186.
- (29) Blöchl, P. E. Projector Augmented-Wave Method. *Phys. Rev. B* **1994**, *50*, 17953–17979.
- (30) Perdew, J. P.; Burke, K.; Ernzerhof, M. Generalized gradient approximation made simple. *Phys. Rev. Lett.* **1996**, *77*, 3865–3868.
- (31) Monkhorst, H. J.; Pack, J. D. Special Points for Brillouin-Zone Integrations. *Phys. Rev. B* **1976**, *13*, 5188–5192.
- (32) Sun, K.; Zhao, Y.; Su, H. Y.; Li, W. X. Force Reversed Method. or Locating Transition States. *Theor. Chem. Acc.* **2012**, *131*, 1–10.
- (33) Henkelman, G.; Uberuaga, B. P.; Jónsson, H. A Climbing Image Nudged Elastic Band Method for Finding Saddle Points and Minimum Energy Paths. *J. Chem. Phys.* **2000**, *113*, 9901–9904.
- (34) Henkelman, G.; Jónsson, H. Improved Tangent Estimate in the Nudged Elastic Band Method for Finding Minimum Energy Paths and Saddle Points. *J. Chem. Phys.* **2000**, *113*, 9978–9985.
- (35) Bor, G.; Dietler, U. K. Fundamental Metal Carbonyl Equilibria: A Quantitative Infrared Spectroscopic Study of the Equilibrium between Dicobalt Octacarbonyl and Tetracobalt Dodecacarbonyl under Carbon Monoxide Pressure in Hexane Solution. *J. Organomet. Chem.* **1980**, *191*, 295–302.
- (36) Wang, H.; Zhou, W.; Liu, J. X.; Si, R.; Sun, G.; Zhong, M. Q.; Su, H. Y.; Zhao, H. B.; Rodriguez, J. A.; Pennycook, S. J.; et al. Platinum-Modulated Cobalt Nanocatalysts for Low-Temperature Aqueous-Phase Fischer–Tropsch Synthesis. *J. Am. Chem. Soc.* **2013**, *135*, 4149–4158.
- (37) Liu, J. X.; Su, H. Y.; Sun, D. P.; Zhang, B. Y.; Li, W. X. Crystallographic Dependence of CO Activation on Cobalt Catalysts: HCP versus FCC. *J. Am. Chem. Soc.* **2013**, *135*, 16284–16287.
- (38) Frenking, G.; Fröhlich, N. The Nature of the Bonding in Transition-Metal Compounds. *Chem. Rev.* **2000**, *100*, 717–774.
- (39) Diefenbach, A.; Bickelhaupt, F. M.; Frenking, G. The Nature of the Transition Metal-Carbonyl Bond and the Question about the Valence Orbitals of Transition Metals. A Bond-Energy Decomposition Analysis Of TM(CO)<sub>6</sub>(Q) (Tmq = Hf<sup>–</sup>(–), Ta<sup>–</sup>, W, Re<sup>+</sup>, Os<sup>2+</sup>, Ir<sup>3+</sup>). *J. Am. Chem. Soc.* **2000**, *122*, 6449–6458.
- (40) Dewar, M. A Review of the Pi-Complex. Theory. *Bull. Soc. Chem. Fr.* **1951**, *18*, C71–C79.
- (41) Chatt, J.; Duncanson, L. Olefin Co-Ordination Compounds 0.3. Infra-Red Spectra and Structure - Attempted Preparation of Acetylene Complexes. *J. Chem. Soc.* **1953**, 2939–2947.
- (42) Windham, R.; Bartram, M.; Koel, B. E. Coadsorption of Ethylene and Potassium on Pt(111) 0.1. Formation of a Pi-Bonded State of Ethylene. *J. Phys. Chem.* **1988**, *92*, 2862–2870.